Available online at www.sciencedirect.com
ScienceDirect
Ceramics International 37 (2011) 3515–3521
CERAMICS INTERNATIONAL
www.elsevier.com/locate/ceramint

Preparation and characterization of nanocrystalline La-doped ZnO powders through a mechanical milling and their optical properties

Sumetha Suwanboon [a,*], Pongsaton Amornpitoksuk [b]

[a] Department of Materials Science and Technology, Faculty of Science, Prince of Songkla University, Hat Yai, Songkhla 90112, Thailand
[b] Department of Chemistry and Center for Innovation in Chemistry, Faculty of Science, Prince of Songkla University, Hat Yai, Songkhla 90112, Thailand

Received 27 April 2011; received in revised form 27 May 2011; accepted 3 June 2011
Available online 6 July 2011

Abstract

Structural and optical properties of mechanically milled La-doped ZnO powders are presented in this paper. The $Zn_{1-x}La_xO$ phase formed when x varied in a range of 0.02–0.06 and milled at 400 rpm for 20 h. The secondary La_2O_3 phase occurred with an increase of La content. The crystallite and particle size decreased as a function of La content as x = 0–0.14 due to the effect of Zener pinning and solute drag. The absorption edge shifted to a lower wavelength when La content was increased to x = 0.14 because of the size effect. The energy band gap of $Zn_{1-x}La_xO$ powders varied in a range of 2.96–3.12 eV depending on the crystallite size. The broad emission bands in a visible region centered at about 640 nm are attributed to oxygen deficiency.
© 2011 Elsevier Ltd and Techna Group S.r.l. All rights reserved.

Keywords: A. Powders: solid state reaction; B. X-ray methods; C. Optical properties; D. ZnO

1. Introduction

Nowadays nanostructured materials have an extreme influence on mankinds way of life, as many researchers have been focusing on an investigation of nanostructured materials including preparation, characterization and also elucidating their important properties. Taking into account, first of all, the preparation of nanostructured materials, there are two major approaches for synthesizing nanoparticles. A bottom-up technique is a method of making larger particles from smaller starting materials such as molecules and atoms. This technique usually is concerned with a soft chemical route such as sol–gel, precipitation and hydrothermal method [1]. Another process, a top-down technique is an engineering physics means of making smaller particles from larger starting materials. This technique always consists of grinding, conventional milling and high energy ball milling [1]. Therefore, a selection of the right process for synthesizing nanoparticles can make it possible to produce particles into the desired size and shape. As far as the above methods are concerned, there are no reports to date that reveals a preparation of La-doped ZnO powders by high energy ball milling. On the contrary, a number of metal-doped ZnO powders were investigated, for example; Suwanboon et al. [2] synthesized $Zn_{1-x}Ti_xO$ nanoparticles by milling with a speed of 400 rpm for 20 h. It had been reported that the crystallite size of $Zn_{1-x}Ti_xO$ powders decreased as a function of Ti content and the wider band gap was obtained by increasing the Ti doping content. Marinković et al. [3] reported a preparation of nanocrystalline $ZnCr_2O_4$ spinel structure by milling the starting ZnO and Cr_2O_3 powders in air for 0–320 min. The crystallite size of $ZnCr_2O_4$ was reduced when milling time was increased whereas the strain increased with milling time. Recently, $ZnFe_2O_4$ was prepared [4]. The mixtures of ZnO and Fe_2O_3 powders with a mole ratio of 1:1 were milled at 500 rpm, the $ZnFe_2O_4$ phase appeared after milling for 40 h and the crystallite size and microstrain of resultant products constantly increased. Damonte et al. [5] studied the formation of Al-doped ZnO powders by milling the mixture of Al and ZnO powders from 1 to 16 h. The doping of Al into ZnO induced a depression of crystallization and a shift to lower energy in optical absorption. Karamat et al. [6] prepared $(ZnO)_{1-x}(TMO)_x$ samples, where TM = Mn, Fe and Co by milling for 14 h and the samples showed a red shift in energy band gap for all TM doped-samples.

* Corresponding author. Tel.: +66 74 28 82 50; fax: +66 74 28 83 95.
E-mail address: ssuwanboon@yahoo.com (S. Suwanboon).

0272-8842/$36.00 © 2011 Elsevier Ltd and Techna Group S.r.l. All rights reserved.
doi:10.1016/j.ceramint.2011.06.007

This study, we attempt to prepare $Zn_{1-x}La_xO$ ($x = 0$, 0.04, 0.06, 0.10, 0.14 and 0.20) by high energy ball milling. The effect of milling time and La-doping content on crystallite size were realized as well as the dependence of optical properties on La content was also investigated.

2. Experimental

The starting materials are ZnO (99%, Fluka Chemie, Switzerland) and La_2O_3 (99.98%, Sigma–Aldrich, USA) powders. $Zn_{1-x}La_xO$ powders were prepared by the Pulverisette 7 FRITSCH planetary ball mill. The stoichiometric quantities were weighted to obtain mixtures of ZnO with 2, 6, 10, 14 and 20 mol% of La or $x = 0$, 0.04, 0.06, 0.10, 0.14 and 0.20. The milling was performed in a silicon nitride vial with silicon nitride balls (10 mm in diameter) in air during 1, 5, 10 and 20 h. The ball-to-powder mass ratio (BPR) was kept at 10:1 and the speed was 400 rpm. The mixtures were milled for 10 min, alternating with a stop for 5 min so as to prevent over heating. In this study, the silicon nitride vial and silicon nitride balls were used so as to prevent an impurity of the product that might come from inappropriate vial and balls.

The X-ray powder diffraction data of the milled samples were recorded using an X-ray diffractometer (XRD, X'Pert MPD, PHILIPS). The morphology of milled samples was observed by a scanning electron microscope (SEM, QUANTA 400, FEI) and transmission electron microscope (TEM, JEM-2010, JEOL). Diffuse reflection spectra (DRS) were recorded by a UV–vis spectrophotometer (UV-vis 2450, Shimadzu). Room temperature photoluminescence (PL) spectra were measured by a luminescence spectrometer (LS/55, PerkinElmer).

3. Results and discussion

3.1. Effect of milling time

In this study, $Zn_{0.80}La_{0.20}O$ was selected as a representative sample to investigate the effect of milling time on phase formation. The mixture of 0.6516 g (20 mol%) La_2O_3 and 1.4648 g ZnO powders was milled for 1, 5, 10 and 20 h and X-ray diffraction patterns of all milled samples are presented in Fig. 1.

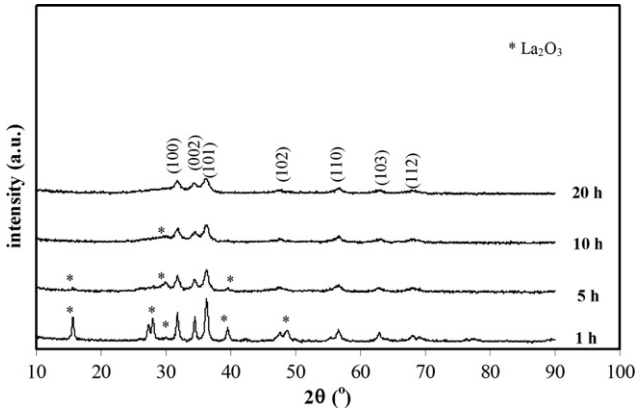

Fig. 1. XRD patterns of $Zn_{0.80}La_{0.20}O$ powders after different milling times.

The diffraction peaks of starting La_2O_3 powders were clearly observed in a pattern of the samples milled at 1, 5 and 10 h and then disappeared after milling for 20 h. The absence of the La_2O_3 peaks implied that the solid solution of La-doped ZnO powders with a hexagonal structure compared to the JCPDS card number 36-1451 could completely be formed. By the planetary milling method, the high impact force was introduced to the milling system and the temperature was then further increased whilst the milling time was increased, giving rise to an easy diffusion of La ions into the ZnO structure as occurred in the case of Ti-doped ZnO powders [2]. It has been well documented that the mechanical milling is an important technique for reducing the particle size of solid material and producing a solid solution. It can be observed from Fig. 1 that a broadening with a low intensity of diffraction peaks is detected when milling time was increased, indicating that the crystallite size decreased. In this investigation, the crystallite size and lattice strain of the major phase were evaluated by the Williamson–Hall equation [2]:

$$\frac{\beta\cos\theta}{\lambda} = \frac{k}{d} + \frac{\eta\sin\theta}{\lambda} \quad (1)$$

where β is the full-width at the half maximum (FWHM) of the diffraction peak, θ is the Bragg angle, λ is the wavelength of X-ray used, d is the average crystallite size, k is a constant ($k = 0.9$) and η is a lattice strain. The results are presented in Table 1.

Based on Table 1, the crystallite size decreased as a function of milling time. The crystallite size diminished very rapidly at the beginning to 10 h of milling and still decreased slightly with further milling up to 20 h. The reduction of crystallite size at the same time as increasing the milling time is due to the fact that mixtures are more fractured than rewelded during the collision between the mixtures and milling media [2]. Unlike the crystallite size change, the lattice strain increased when milling time was increased. Due to the high energy impact, the lattice strain led to produce a number of lattice imperfections such as dislocations and other defects [2,4], bringing about the formation of lattice strain. Therefore, the lattice strain can be produced in greater quantity when the nanoparticles have a more defect concentration.

3.2. Effect of La content

The effect of La content on $Zn_{1-x}La_xO$ ($x = 0$, 0.02, 0.06, 0.10, 0.14 and 0.20) formation was studied. After the mixtures

Table 1
Effect of milling time on the crystallite size and lattice strain of $Zn_{0.80}La_{0.20}O$ powders.

Milling time (h)	Crystallite size (nm)	Lattice strain
1	33.5	0.95
5	29.2	1.04
10	22.0	1.44
20	17.7	1.68

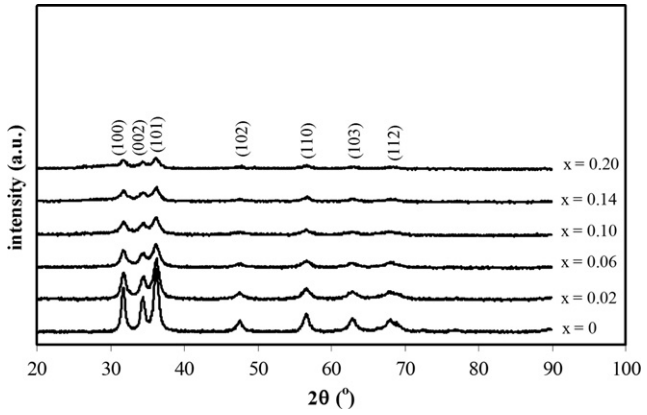

Fig. 2. XRD patterns of as-milled $Zn_{1-x}La_xO$ powders.

were milled with a speed of 400 rpm for 20 h, the crystalline phase of as-milled powders were determined by XRD technique and all XRD results are displayed in Fig. 2.

The XRD patterns of the milled $Zn_{1-x}La_xO$ samples did not show any peaks of secondary phases such as La_2O_3 within the detection limit of X-ray diffraction used. The peak intensities decreased whereas the widths of the XRD lines increased as doping content (x) was increased to 0.14. As $x > 0.14$, the peak intensities and the width of XRD lines changed inversely as observed in $x \leq 0.14$. As in our previous study [2], the broader lines were observed when higher Ti doping content was used because of the reduction of crystallite size. Alike, the change in peak broadening and peak intensities as a function of La content can be explained by the diminutive crystallite size. Therefore, the crystallite size was calculated through the Scherrer's equation [7] so as to confirm the above mentioned results.

$$d = \frac{0.9\lambda}{\beta \cos\theta} \tag{2}$$

where d is the crystallite size of the milled samples, θ is the peak position, λ is the X-ray wavelength and β is the full-width at half maximum of the XRD lines. In like manner, the change in lattice parameters a and c was also estimated using (1 0 0) and (0 0 2) planes of the milled samples according to the following relationship:

$$\frac{1}{d_{hkl}^2} = \frac{4}{3}\left(\frac{h^2 + hk + k^2}{a^2}\right) + \frac{l^2}{c^2} \tag{3}$$

where $d_{h\,k\,l}$ is the lattice spacing of the (h k l) plane and a and c are the lattice parameters. The calculated crystallite size and lattice parameters are presented in Table 2

It is evident that the materials in a nanometer scale have a large surface area and surface energy of the system. Therefore, a simple relaxation (expansion or contraction) of the crystalline lattice may lead to stabilization of metastable nanostructure. The change in lattice parameter of metal-doped ZnO powders is dependent upon the ionic radius of doping ion, which can substitute the Zn ion in the lattice. When doping ion that has a smaller ionic radius compared to Zn ion is substituted the Zn site in ZnO lattice, the lattice parameters decrease [8]. In contrast, when doping ion that has a bigger ionic radius

Table 2
The properties of as-milled $Zn_{1-x}La_xO$ powders.

x	Crystallite size (nm)	Lattice parameter (nm)		E_g (eV)
		a	c	
Bulk ZnO	57.3	0.3248(6)	0.5204(1)	–
0	22.2	0.3259(3)	0.5222(0)	2.96
0.02	19.4	0.3252(3)	05212(8)	3.03
0.06	18.5	0.3260(7)	0.5214(9)	3.05
0.10	17.4	0.3248(2)	0.5212(0)	3.06
0.14	16.5	0.3248(0)	0.5201(6)	3.12
0.20	17.7	0.3253(4)	0.5233(6)	3.08

compared to Zn ion is substituted into Zn site, the lattice parameters increase [9]. Taking into account the revealed ionic radius, the ionic radii of La^{3+} and Zn^{2+} ion are 0.106 nm and 0.074 nm, respectively. Therefore, when the La ions systematically are substituted for the Zn sites, the lattice parameters of the La-doped ZnO powders expand. Under the certain experiments, the lattice parameters increased linearly compared to bulk ZnO powders when the La content varied in a range of $x = 0.02$–0.06. This evidence indicated that the samples form a solid solution as $Zn_{1-x}La_xO$ ($x = 0.02$–0.06) [9]. As $x = 0$, the lattice parameters are larger than those of the $Zn_{1-x}La_xO$ ($x = 0.02$–0.06) powders due to the presence of higher defect concentration such as oxygen vacancies, giving rise to an increase in lattice parameters of milled ZnO powders. On the other hand, the lattice parameters decreased when La content is between of $x = 0.10$–0.14. This evidence was also observed in the report [10], but the authors did not explain why the lattice parameters were contracted instead of expansion. In this study, we theoretically imagined that the amorphous phase of La_2O_3 could exist as reported [11] due to the solubility limit of La ions in ZnO structure. Thus, small La_2O_3 clusters were dispersed uniformly on the surface of ZnO powders and compressed the crystal lattice of ZnO to cause the contraction of the lattice parameters as occurring in Ti-doped MgO powders [12]. However, the lattice parameters increased suddenly when the La content was increased to $x = 0.20$, this might be due to the abnormal grain growth that is shown in Table 2 and Fig. 4(f).

The reduction of crystallite size can be explained by the effects of Zener pinning and solute drag. Considering the properties of sample with $x = 0.02$–0.06, the La ions in solid solution of $Zn_{1-x}La_xO$ acted as an impurity or obstacle to prevent the crystal growth due to the effect of Zener pinning. As doping content further increased ($x = 0.10$–0.14), the secondary phase (La_2O_3) presented in the system and this secondary phase also acted as an obstacle to prevent the crystal growth due to the effect of solute drag. When the moving boundaries attach to the obstacles, the retarding force can be then generated and the retarding force per unit area (F_r) can be estimated [7]:

$$F_r = \frac{3 f_r \gamma_b}{2 r_p} \tag{4}$$

where f_r is the number of obstacles per unit volume, γ_b is the grain boundary energy and r_p is the obstacle radius. In general,

small crystals or minute particles form a metastable phase, so these crystals or particles grow in order to reduce the overall energy and the driving force for growing is defined as:

$$F_d = \frac{\alpha\gamma_b}{r} \quad (5)$$

where r is the particle radius, γ_b is the grain boundary energy and α is a geometrical constant. As a matter of fact, the presence of a greater retarding force produced a greater inhibition of the crystal growth. Considering Eq. (4), the number of obstacles per unit volume (f_r) is the major parameter influencing the increment of retarding force for inhibiting the crystal growth. In this case study, the substitutional La ions at the Zn sites and La_2O_3 adsorbed on ZnO surface formed more and more when the concentration of La ions in the solutions was greater than before. For this reason, the crystallite size diminished when the greater substitutional La and La_2O_3 formed. However, when the La content was further increased to $x = 0.20$, the crystallite size of La-doped ZnO powders increased again because of the efficiency of pinning was reduced due to the coarsening of the obstacle, bringing about the change in f_r/r_p ratio as a result of an increase in r_p as described in our previous attempt [7]. To confirm that a small amount of amorphous La_2O_3 presented when doping with large amount of La content, the La-doped ZnO powders were annealed at 600 °C in air for 1 h. Then, the crystalline phase of annealed La-doped ZnO powders were identified using an X-ray diffraction technique and the results are shown in Fig. 3.

Low diffraction intensity of La_2O_3 peaks was observed in the XRD pattern of annealed samples when $x > 0.10$. So, it can be concluded that amorphous La_2O_3 powders really formed and adsorbed on ZnO surface during milling process as previously predicted. Fig. 4(a)–(f) shows a secondary electron image of La-doped ZnO particles. It was noticed that small irregular particles with a size of approximately a few hundred nanometers aggregated and became a cluster of particles. The particle size observed from SEM images is somewhat similar except the ZnO powders doping with 20 mol% La (Fig. 4(f)), the particle size increased again in accordance with the crystallite size obtained from XRD investigation. TEM image of ZnO powders doping with 14 mol% La were demonstrated in Fig. 4(g). It was observed that the particle size varied in a range of 100–200 nm.

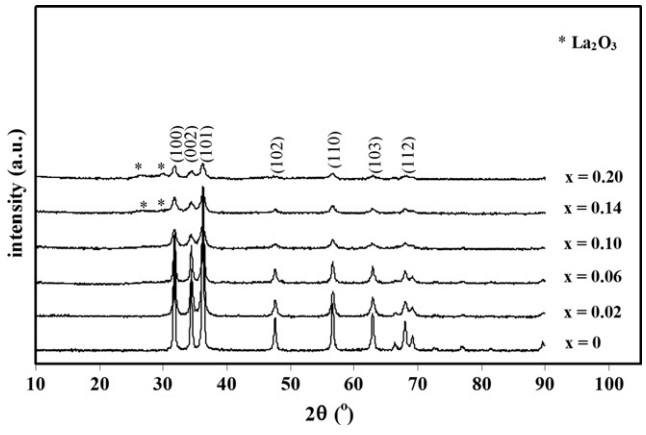

Fig. 3. XRD patterns of annealed $Zn_{1-x}La_xO$ powders at 600 °C.

3.3. Dependence of E_g value on La content

In this analysis, the absorption spectra of La-doped ZnO powders were recorded and depicted in Fig. 5. It was clearly observed that the absorption edge of all La-doped ZnO powders shifted to a shorter wavelength or higher energy when the La content was varied between $x = 0$–0.14, this can be explained by the size effect [13].

To estimate the value of band gap, the curve of $(\alpha E)^2$ versus E (where α is an absorption coefficient and E is the photon energy) [14] was plotted as shown in Fig. 6.

The energy band gap of the milled La-doped ZnO powders was determined by the extrapolation of the straight line down to zero on the x-axis (where $E = E_g$) and the results are shown in Table 2. As a matter of fact, ZnO is an n-type semiconducting compound with a wide band gap of 3.2 eV [2] that can be used in many optoelectronic devices [15]. The E_g value of ZnO powders altered depending on many parameters, for example, imperfection in ZnO crystal [14], particle shape [14] and particle size [13]. In this investigation, the E_g value of La-doped ZnO powders was dependent upon the crystallite size. The E_g value increased as a function of La content until $x = 0.14$ because the crystallite size decreased. But the E_g value decreased when La content was further increased to $x = 0.20$, resulting from the increase in crystallite size.

In this study, the room temperature PL of as-milled La-doped ZnO powders was recorded in a wavelength of 450–800 nm and the spectra are presented in Fig. 7; a visible broad band centered at about 640 nm can be detected. It was observed that a broad visible emission occurred between the wavelength of 450–800 nm usually originating from many defects such as zinc vacancy, zinc interstitial, oxygen vacancy and oxygen interstitial [16]. In general, as-milled samples with higher emission intensity occupy higher defect concentration. From this viewpoint, the defects can generate the energy levels within the forbidden zone of the samples, thus electrons can transit between the filled valence band and the energy level of defects, giving rise to a narrower E_g value obtained with respect to the single ZnO crystal. The emission intensity of as-milled ZnO powders is higher than the emission intensity of all La-doped ZnO powders. This effect can influence a reduction of E_g value of as-milled ZnO powders. As noted, in room temperature PL spectra, the emission intensity of as-milled La-doped ZnO powders decreased systematically when La content (x) was varied in a range of 0.06–0.20, but $Zn_{0.98}La_{0.02}O$ powders exhibited a lower intensity compared to the other La-doped ZnO powders, this might be due to a decrease of the active centers responsible for this band [17]. Therefore, the enhancement of E_g value of La-doped ZnO powders in this investigation was strongly promoted by a reduction of crystallite size as previously mentioned.

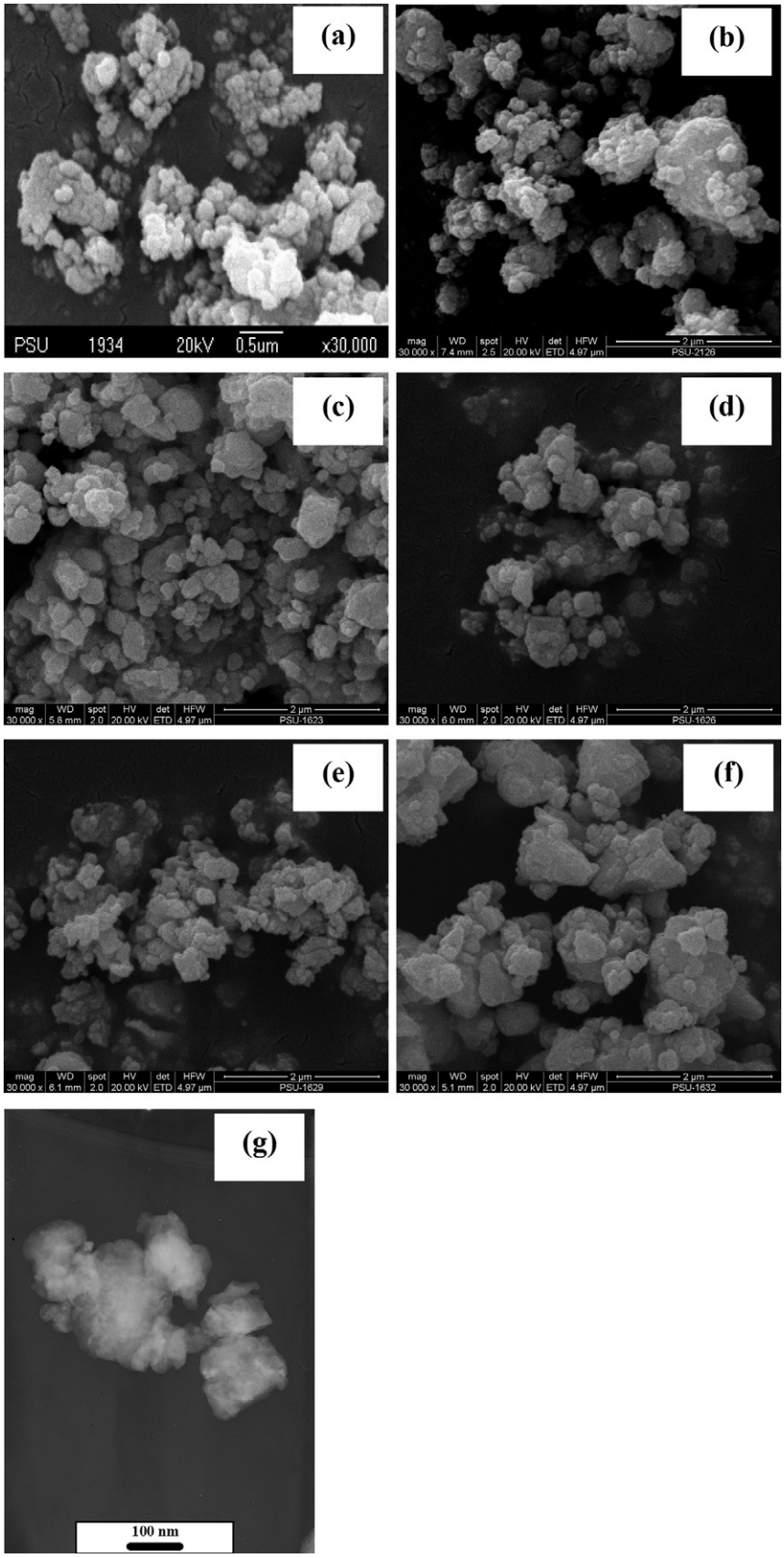

Fig. 4. SEM images of as-milled $Zn_{1-x}La_xO$ powders where (a) $x = 0$, (b) $x = 0.02$, (c) $x = 0.06$, (d) $x = 0.10$, (e) $x = 0.14$ and (f) $x = 0.20$ as well as a TEM image of as-milled $Zn_{1-x}La_xO$ powders where (g) $x = 0.14$.

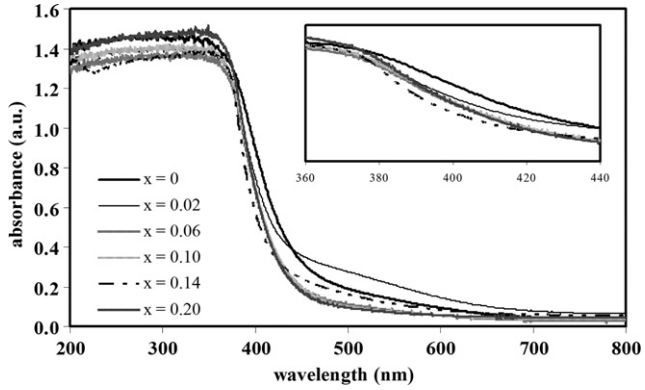

Fig. 5. The absorption spectra of as-milled La-doped ZnO powders at different La contents.

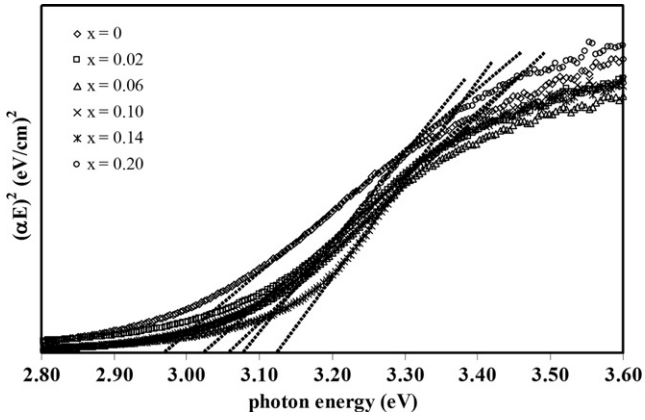

Fig. 6. Plots of $(\alpha E)^2$ versus photon energy (E) of as-milled La-doped ZnO powders at different La contents.

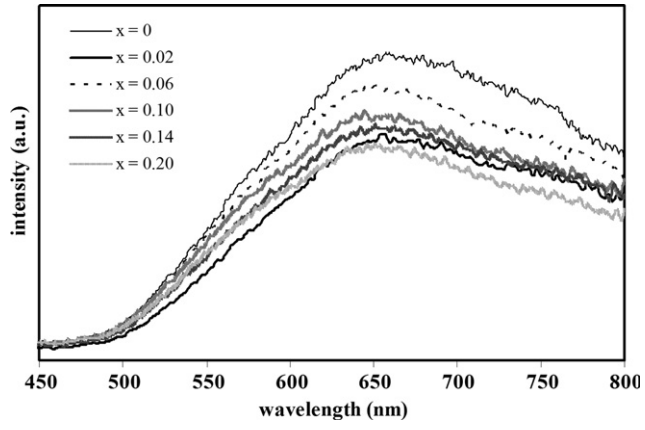

Fig. 7. Room temperature PL spectra of as-milled La-doped ZnO powders at different La contents.

4. Conclusions

Mechanical milling is a powerful technique for synthesizing La-doped ZnO powder because high impact energy transpired in a fracture of large particles and produced small particles in a nanoscale level. The La-doped ZnO powder occurred by milling at a speed of 400 rpm for 20 h. The La ions can substitute into the Zn sites as $x \leq 0.06$. As $x > 0.06$, the secondary La_2O_3 phase was present and this evidence was confirmed by XRD results of annealed La-doped ZnO powders at 600 °C. The reduction of crystallite size as a function of La content can be explained by the Zener pinning and solute drag effects. The enhancement of E_g value was promoted by a decrease in crystallite size. The emission intensity in the visible range of as-milled powders decreased when La content was increased expect when $x = 0.02$ because of a decrease of the active centers of $Zn_{0.98}La_{0.02}O$ powder.

Acknowledgements

This work has been supported by Science Research Fund, Faculty of Science, Prince of Songkla University (Fiscal Year 2011) under the Contact Number 154001. The authors also would like to acknowledge the Center for Innovation in Chemistry (PERCH-CIC), Commission on Higher Education, Ministry of Education and the authors would like to acknowledge Michael Benjamin Lane for his English manuscript proofreading service.

References

[1] G.A. Ozin, A.C. Arsenault, L. Cademartiri, Nanochemistry: A Chemical Approach to Nanomaterials, second ed., RCS Publishing, Cambridge, 2009
[2] S. Suwanboon, P. Amornpitoksuk, P. Bangrak, Synthesis, characterization and optical properties of $Zn_{1-x}Ti_xO$ nanoparticles prepared via a high-energy ball milling technique, Ceram. Int. 37 (2011) 333–340.
[3] Z.V. Marinković, L. Mančić, P. Vulić, O. Milošević, Microstructural characterization of mechanically activated Zn–Cr_2O_3 system, J. Eur. Ceram. Soc. 25 (2005) 2081–2084.
[4] Z.W. Zhao, K. Ouyang, M. Wang, Structural macrokinetics of synthesizing $ZnFe_2O_4$ by mechanical ball milling, Trans. Nonferrous Met. Soc. China 20 (2010) 1131–1135.
[5] L.C. Damonte, V. Donderis, M.A. Hernández-Fenollosa, Trivalent dopants on ZnO semiconductor obtained by mechanical milling, J. Alloys Compd. 483 (2009) 442–444.
[6] S. Karamat, C. Ke, T.L. Tan, W. Zhou, P. Lee, R.S. Rawat, Investigation of impurity phase formation for $(ZnO)_{1-x}(TMO)_x$ bulk samples formed by ball milling, Appl. Surf. Sci. 255 (2009) 4814–4820.
[7] S. Suwanboon, P. Amornpitoksuk, A. Sukolrat, Dependence of optical properties on doping metal, crystallite size and defect concentration of M-doped ZnO nanopowders (M = Al, Mg, Ti), Ceram. Int. 37 (2011) 1359–1365.
[8] M. Farbod, M.Z. Shoushtari, S. Parhoodeh, Fabrication and characterization of $Zn_{1-x}Al_xO$ nanoparticles by DC arc plasma, Physica B 406 (2011) 205–210.
[9] B.N. Dole, V.D. Mote, V.R. Huse, Y. Purushotham, M.K. Lande, K.M. Jadhav, S.S. Shah, Structural studies of Mn doped ZnO nanoparticles, Curr. Appl. Phys. 11 (2011) 762–766.
[10] T. Jia, W. Wang, F. Long, Z. Fu, H. Wang, Q. Zhang, Fabrication, characterization and photocatalytic activity of La-doped ZnO nanowires, J. Alloys Compd. 484 (2009) 410–415.
[11] S. Anandan, A. Vinu, K.L.P. Sheeja Lovely, N. Gokulakrishnan, P. Srinivasu, T. Mori, V. Murugesan, K. Ariga, Photocatalytic activity of La-doped ZnO for the degradation of monocrotophos in aqueous suspension, J. Mol. Catal. A: Chem. 266 (2007) 149–157.
[12] W. Wang, X. Qiao, J. Chen, F. Tan, H. Li, Influence of titanium doping on the structure and morphology of MgO prepared by coprecipitation method, Mater. Charact. 60 (2009) 858–862.
[13] S. Suwanboon, P. Amornpitoksuk, S. Muensit, Enhancement of optical bandgap and luminescent characteristics of one-dimensional ZnO nanoparticles, J. Ceram. Process. Res. 11 (2010) 419–424.

[14] S. Suwanboon, P. Amornpitoksuk, P. Bangrak, A. Sukolrat, N. Muensit, The dependence of optical properties on the morphology and defects of nanocrystalline ZnO powders and their antibacterial activity, J. Ceram. Process. Res. 11 (2010) 547–551.
[15] C.Y. Hsu, C.H. Tsang, Effects of ZnO buffer layer on the optoelectronic performances of GZO films, Solar Energy Mater. Solar Cells 92 (2008) 530–536.
[16] N. Samaele, P. Amornpitoksuk, S. Suwanboon, Effect of pH on the morphology and optical properties of modified ZnO particles by SDS via a precipitation method, Mater. Lett. 6 (4) (2010) 500–502.
[17] L.C. Damonte, L.A. Mendoza Zélis, B. Mari Soucase, M.A. Hernández Fenollosa, Nanoparticles of ZnO obtained by mechanical milling, Powder Technol. 14 (8) (2004) 15–19.